Dual function for Tango1 in secretion of bulky cargo and in ER-Golgi morphology

Supporting Information Appendix

Materials and Methods

Fly stocks and genetics

All experiments were done at 25ºC in standard conditions. To generate homozygous mutant *tango1* terminal cells we used the MARCM system (1), with the lines *hsFlp1.22; tub-GAL80, FRT40A; btl-GAL4, UAS-eGFP* (from Stefan Luschnig, University of Muenster, Germany), and the line *FRT40A* as control (Bloomington Drosophila Stock Center [BDSC] #5615). *2L3443* was mapped by complementation tests with *Df(2L)BSC7* (BDSC #6374), *Df(2L)BSC6* (BDSC #6338) and *Df(2L)BSC187* (BDSC #9672), followed by fine mapping through ORF sequencing of the genes within the segment genetically defined to contain the mutation. Final complementation tests with $tango1^{GS17108}$ (Kyoto Drosophila Genetic Resource Center [DGRC] #206906), and $tango1^{GS15095}$ (DGRC #206078) confirmed 2L3443 as a *tango1* allele.

The lines used as drivers for UAS constructs were *SRF-gal4* (2), *Lpp-gal4* (3), *nub-gal4* (Pastor-Pareja, and Xiu, 2014, #63148), *repo-gal4* (from Christian Klämbt, University of Münster, Germany), and *sr-gal4* (from Frank Schnorrer, Developmental Biology Institute of Marseille (IBDM), France). The following lines were obtained from Vienna Drosophila Resource Center: $ergic53^{fTRG}$ (#318063), $lanA^{fTRG}$ (#318155), $lanB1^{fTRG}$ (#318180) and $BM\text{-}40\text{-}SPARC^{fTRG}$ (#318015), which are fosmid constructs expressing GFP fusion proteins at endogenous levels (4), and *UAS-pio-IR* (#107534). The *UAS-tango1-IR* (#11098R-3) and *UAS-vkg-IR* (#16858R-1) were obtained from the National Institute of Genetics Fly Stock Center, Japan. *dpy-YFP* and *UAS-dpy-IR* are from Barry Thompson, The Francis Crick Institute, UK (5). Collagen-GFP is a protein trap insertion of GFP in the *vkg* locus resulting in a fusion of collagen and GFP (6). $UAS\text{-}crb^{extraTM}\text{-}GFP$ is a construct where the cytoplasmic end of Crb was replaced by GFP (7). *UAS-Gasp-GFP* is from Christos Samakovlis, Stockholm University, Sweden (8). *UAS-Xbp1-GFP* and $UAS\text{-}Xbp1^{spliced}$ is from Pedro Domingos, Nova University of Lisbon, Portugal (9). The following lines were obtained from BDSC: *UAS-GalT-GFP* (#30902), *UAS-ManII-GFP* (#65248), *UAS-RFP-KDEL* (#30910 and #30909), *UAS-mCD8mCherry* (#27392), *UAS-myrRFP* (#63148). *UAS-βPS-Integrin-Venus* was generated by subcloning *βPS-Integrin-Venus* from *pUbi-βPS-Integrin-Venus* [from Guy Tanentzapf, University of British Columbia, Canada (10)] into the *pUASTattB* vector and then inserting in the third chromosome (VK33, BDSC #9750). *UAS-tango1-GFP* was generated by cloning the full-length *tango1* cDNA (GH02877) into pDONR221 (Gateway System, Invitrogen). This was recombined into the destination vectors pTWG from the Drosophila Gateway Vector Collection using the Gateway LR reaction. The construct was then subcloned into *pUASTattB* and injected into VK33.

Whole mount sample preparation, microscopy and analyses

For tracheal terminal cell analyses, third instar wandering larvae were heat-fixed in Halocarbon oil for 30 seconds at 65ºC. For tendon cell analyses, pupae at 24h after puparium formation were hand-peeled and immobilized with heptane glue in MatTek plates with Halocarbon oil. In both cases, samples were imaged immediately using a Zeiss LSM 780 confocal microscope. Quantitative analyses of the number of branching points and air-filling were performed in dorsal terminal cells in metameres 3-6 of heat-fixed larvae. Branches were counted manually in FIJI (11). Analysis of air-filling was performed by visualizing the presence of lumen using light transmission.

Immunofluorescence staining

We used the following antibodies: guinea pig anti-Tango1 (1:400, from Sally Horne-Badovinac, University of Chicago, USA), rabbit anti-Sec16 (1:600, from Catherine Rabouille, Hubrecht Institute, Netherlands), rat anti-Crb (1:500, from Elisabeth Knust, MPI-CBG, Germany), rabbit anti-Pio [1:300, from Markus Affolter, University of Basel, Switzerland (12)], mouse anti-Calnexin99A [1:500, from Sean Munro, MRC, UK (13)] mouse anti-βPS Integrin (1:200, DSHB #6G11), rabbit anti-Sec23 (1:200, Thermo Scientific #PA1-069), rabbit anti-GM130 (1:500, Abcam #ab30637), and rabbit anti-Dof [1:200 (14)]. Alexa-conjugated antibodies from Thermo Scientific: Alexa568 goat anti-mouse (A-11031), Alexa568 goat anti-rat (A-11077), Alexa647 goat anti-rat (A-21247), Alexa568 goat anti-rabbit (A-11036), Alexa647 goat anti-rabbit (A-21245), Alexa568 goat anti-guinea pig (A-11075), Alexa647 goat anti-guinea pig (A-21450). Chromotek's GFP-booster coupled to Atto488 (gba488) and RFP-booster coupled to Atto594 (rba594) were used to enhance signal from fluorescent reporters.

Third instar wandering larvae were collected, dissected, fixed using 4% PFA in PBS for 20 min and washed with PBTx (0.3% Triton X-100 in PBS) followed by 1 h incubation in blocking solution (PBTx, 1% BSA). Primary antibodies were diluted in blocking solution and incubated overnight at 4°C. After washing with PBTx, samples were incubated with secondary antibodies diluted in blocking solution at room temperature for 90 min followed by extensive washing using PBTx. Samples were mounted for imaging using Vectashield with DAPI (Vector Laboratories) and images acquired on Leica SP2, Zeiss LSM 780 or Zeiss LSM 880 Airyscan confocal microscopes.

Western blotting

We used guinea pig anti-Tango1 (1:10,000, mentioned above) and mouse anti-βTubulin (1:5000, Amersham Life Science). HRP-conjugated antibodies were from Jackson ImmunoResearch Laboratories: goat anti-guinea pig-HRP (106-035-003) and goat anti-mouse-HRP (115-035-003). For each genotype, 20 embryos were selected, homogenized in loading buffer and heated for 5 min at 95°C. Samples were then separated by SDS-PAGE, transferred to PVDF membranes and subjected to immunodetection using the Luminata Crescendo Western HRP system.

Image analyses

All analyses were done using FIJI unless specified. We determined the amount of collagen surrounding terminal cells by quantifying the fluorescence intensity of collagen-GFP at the cell membrane close to the terminal cell body. We subtracted the background from the mean fluorescence intensity of an area of 3 x 30 pixels within a single confocal plane. To determine Sec16 and Sec23 particle size and number, and Dpy and laminin accumulation, we masked the channel of interest with the contour of the cell or tissue of interest, and then segmented individual dots from maximum projection images. For Dpy, Sec23 and Calnexin amount in wing discs, we used the plot profile function. To determine the amount of ERGIC53-GFP within ERES, Sec16 dots were segmented in 3D using Imaris and the amount of ERGIC53 within each dot was quantified. We analysed the degree of colocalization of Calnexin and cargo proteins by using the Coloc2 module from FIJI. For this, the theoretical point spread function was calculated using Nyquist tool. The intensity of the generated PSF was measured and the distance between points with half the intensities was calculated and used for analyses. All images within an experiment were acquired using the same microscope settings. Where noted, images were deconvolved using Huygens Remote Manager Software.

Statistical analyses

We used GraphPad Prism 6 for all statistical analyses. Plots were generated using GraphPad Prism 6 or Microsoft Excel.

Supporting Figures

Figure S1. Molecular defects in *tango1*^{2L3443}.

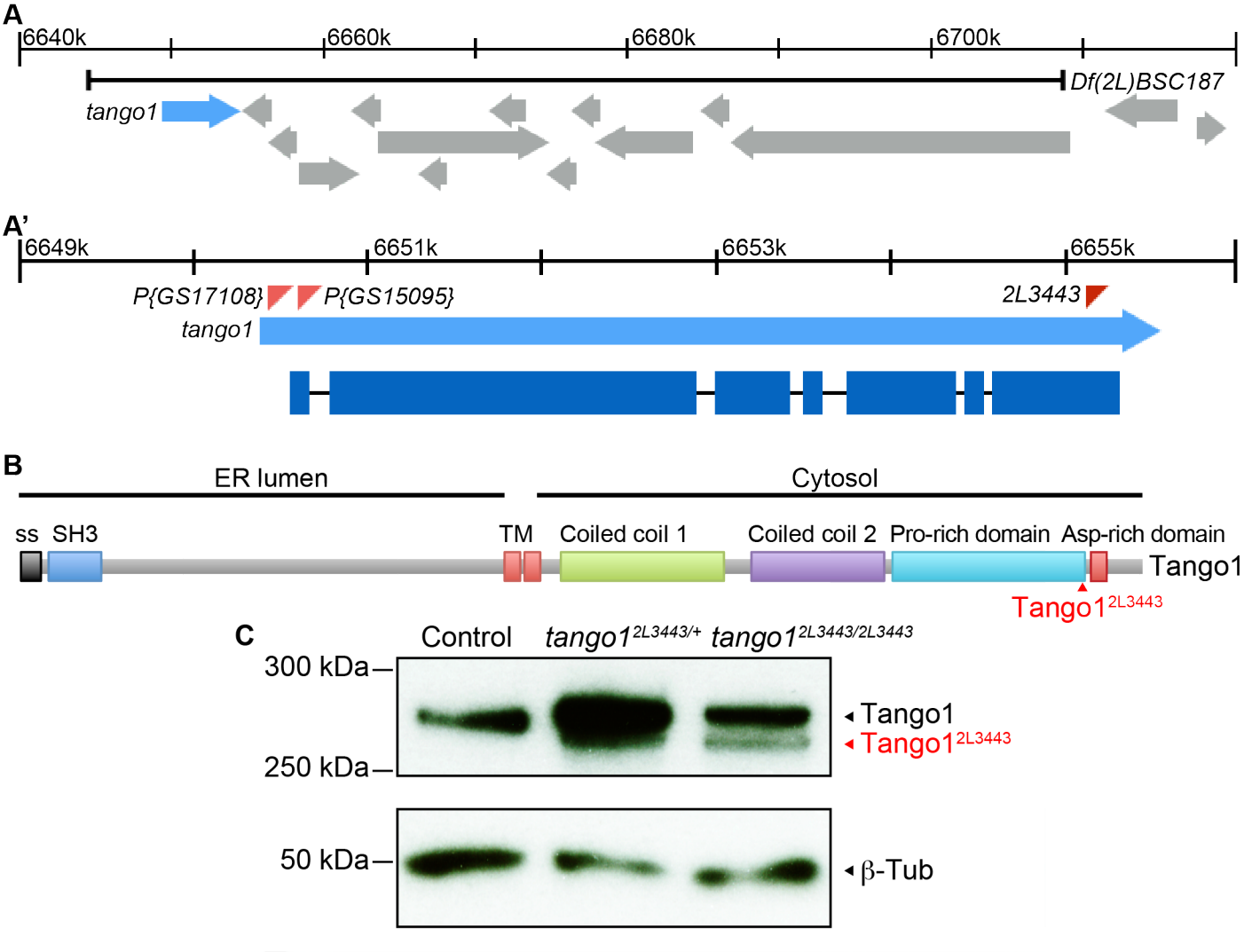

(A) Schematic representation of the *tango1* locus including the extent of deficiency Df(2L)BSC187, which was among those used to map the *tango1*^{2L3443} mutation. (A') Higher resolution of the *tango1* gene and its coding sequence, the positions of the mutation in *2L3443* allele, and P-element insertions in two other *tango1* alleles used for complementation tests. (B) Domain composition of Tango1 and position of the truncation in the protein encoded by *tango1*^{2L3443}. (C) A lower molecular weight protein is seen in *tango1*^{2L3443} homozygous mutant embryos. The higher molecular weight band is likely to be maternally deposited Tango1 wild type protein.

Figure S2. Effects of loss of Tango1 in ER, Golgi and COPII organization

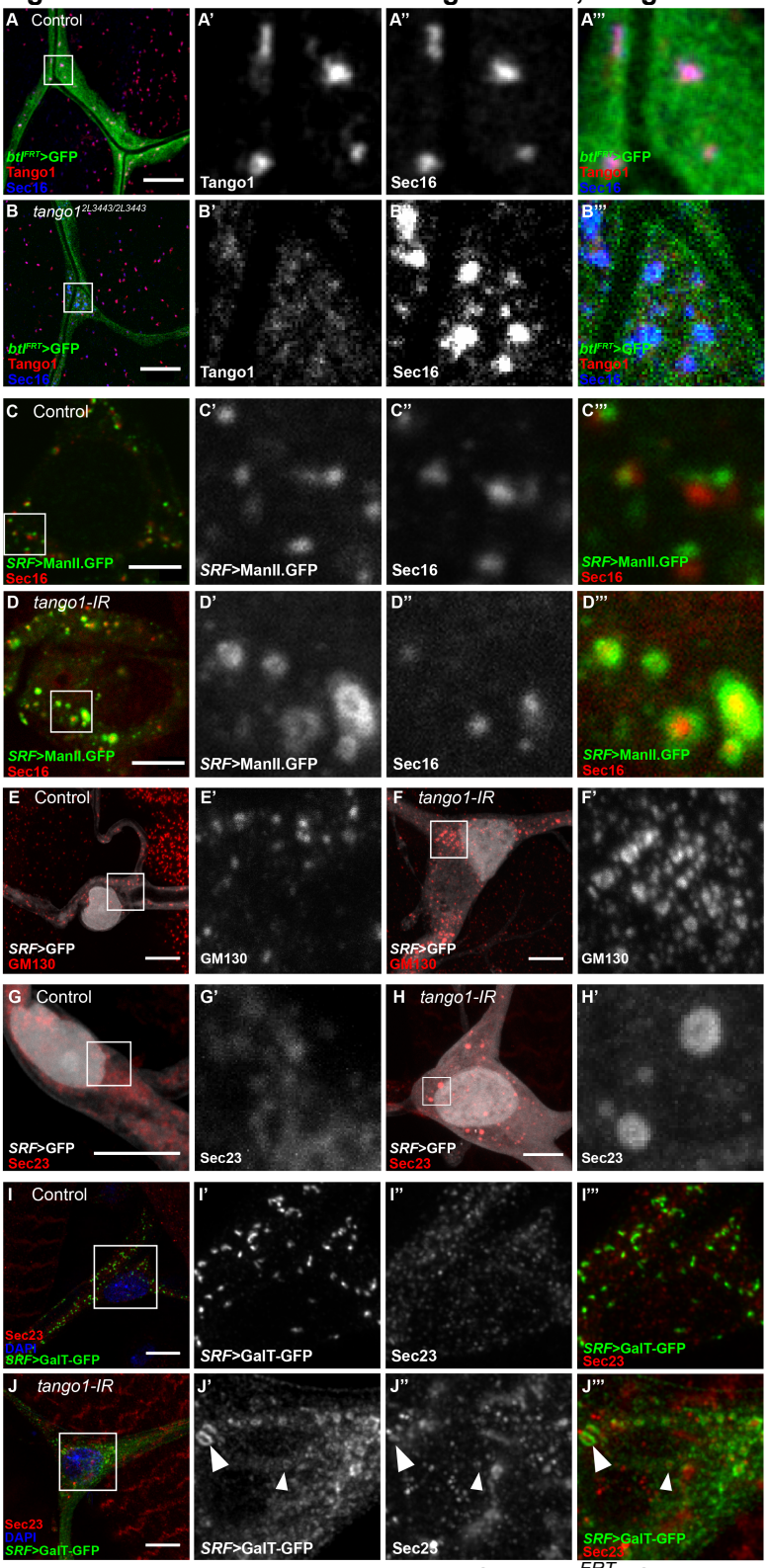

(A-B) Mutant clonal cells expressing GFP (*btl*^{FRT}>GFP) were stained for Tango1 and Sec16. In control cells (A), Tango1 and Sec16 colocalize. In mutant clones Tango1^{2L3443} distribution no longer coincides with that of Sec16, which also forms heterogeneous aggregates (B). (C-D) Terminal cells expressing the Golgi marker Mannosidase II fused to GFP (ManII-GFP) under *SRF-gal4*, and stained for Sec16. (C) In control cells ManII-GFP and Sec16 are juxtaposed, whereas in the absence of *tango1*, ManII-GFP encloses Sec16 (D). (E-F) Terminal cells expressing GFP under *SRF-gal4* and stained for GM130. Control cells show a GM130 punctate distribution (E). *tango1* knockdown cells show GM130 aggregates (F). (G-H) High magnification images of terminal cells expressing GFP under *SRF-gal4* and stained for Sec23. In control cells, Sec23 shows a punctate distribution throughout the cytoplasm, whereas in cells lacking Tango1 it forms ring-like structures. (I-J) Terminal cells expressing the Golgi targeting sequence of Beta-1,4-galactosyltransferase fused to GFP (GalT-GFP) under *SRF-gal4*, and stained for Sec23. (I) In control cells GalT-GFP and Sec23 are dispersed in the cytoplasm, whereas in the absence of *tango1*, GalT-GFP encloses Sec23 (J).Scale bars are 10μm (A-B, E-J) and 5 μm (C-D).

Figure S3. Effects of collagen depletion in tracheal cells and fat body

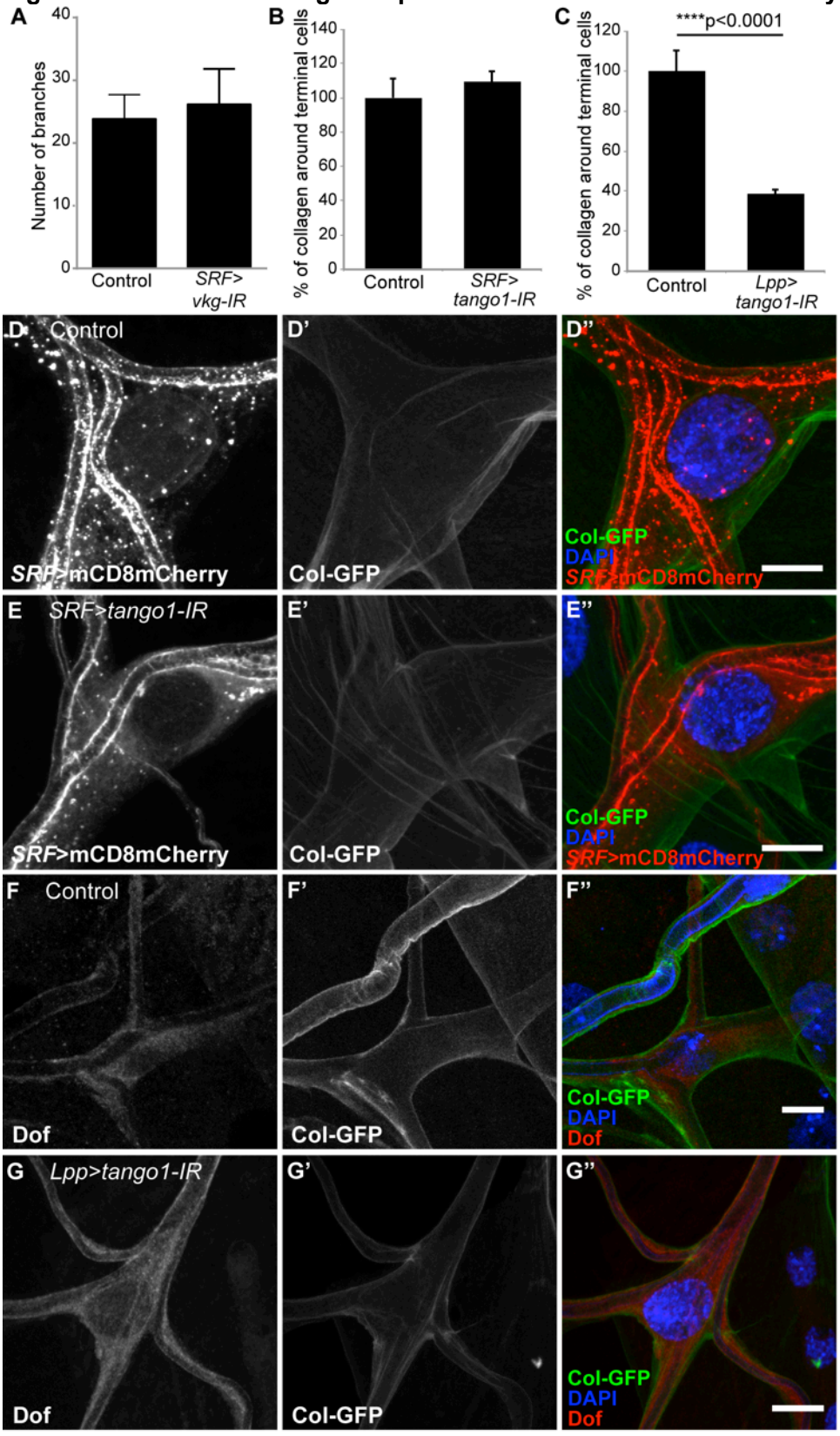

(A) Terminal cells expressing RNAi against *vkg,* which codes for collagen, show no reduction in branch number compared to controls. Control, n=8; *tango1-IR,* n=13. (B) Collagen-GFP surrounding terminal cells was quantified after *tango1-IR* expression in terminal cells using *SRF-gal4*. Control, n=12; *tango1-IR*, n=15. (C) Collagen-GFP surrounding terminal cells was quantified after *tango1-IR* expression in fat body using *Lpp-gal4*. Control, n=15, *tango1-IR,* n=15. Significance was assessed using two-tailed t-test. (D-G) Representative images of control (D) and *tango1* knockdown in terminal cells (E), and of control (F) and *tango1* knockdown in fat body (G). In (F, G) staining against Dof allows visualization of the terminal cell. Col-GFP (collagen-GFP) is a GFP insertion in the *vkg* gene that results in the collagen–GFP fusion being expressed at endogenous levels. Bars in (A-C) represent mean +/-SD. Scale bars in (D-G) are 10μm.

Figure S4. Cargo accumulation and ER defects in wing disc, glial and tendon cells.

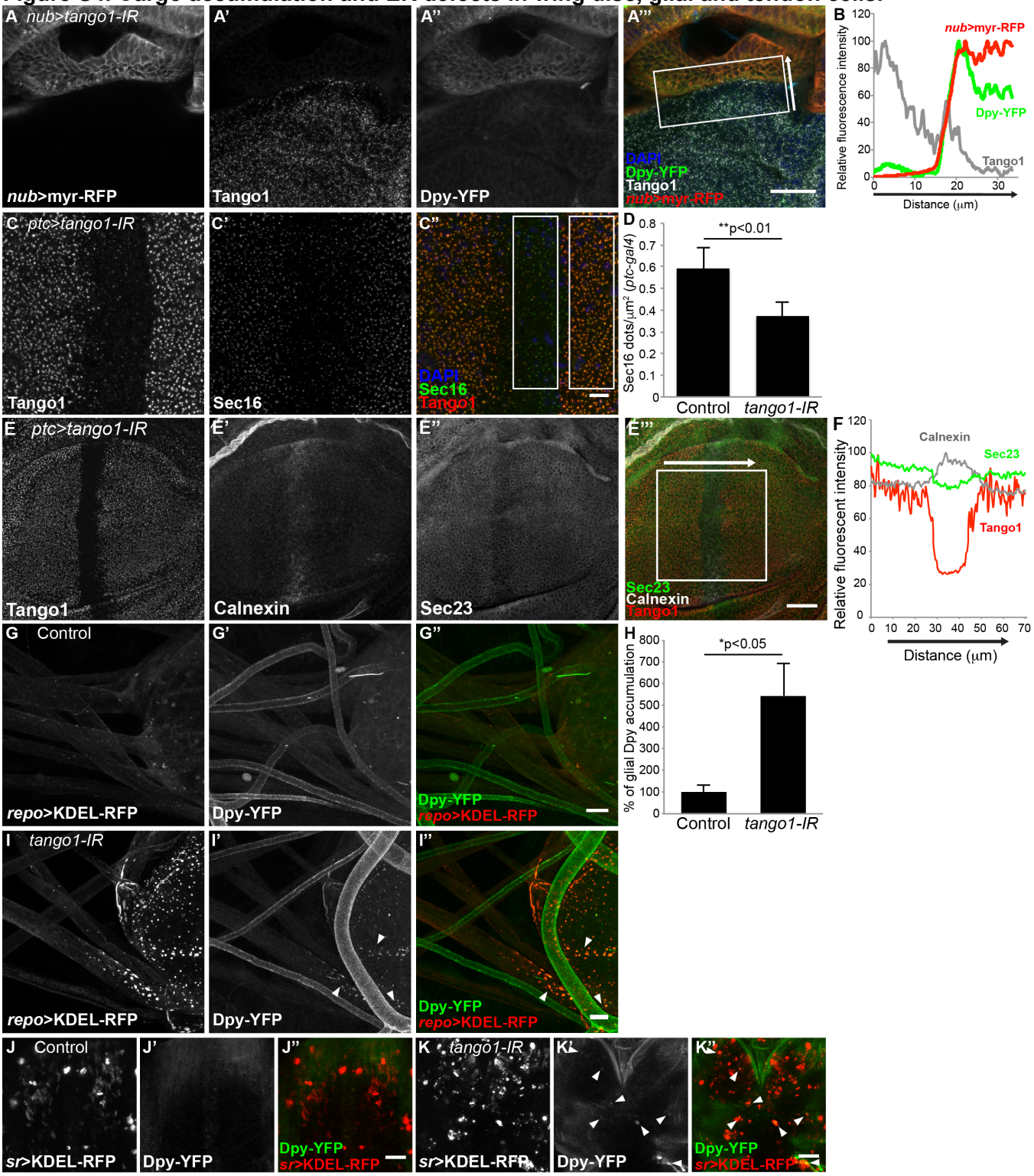

(A) Wing disc from animals with an endogenously tagged Dpy protein (Dpy-YFP) expressing myr-RFP and *tango1-IR* in the wing pouch under *nub-gal4*. Tango1 was stained to confirm the efficiency of knockdown. (B) Intensity profile in the direction of the white arrow and summed across the width of the box in (A). (C, E) Wing discs expressing *tango1-IR* under the *ptc-gal4* driver and stained for Sec16 (C) or Sec23 and Calnexin (E). Absence of Tango1 staining reveals the region where *tango1-IR* is expressed. (D) The number of Sec16 dots (+/- SD) in the boxed regions in (C''). (F) Intensity profile in the direction of the white arrow summed across the width of the box in (E). (G-I) Larval brains expressing KDEL-RFP as an ER marker under the glial-specific driver *repo-gal4.* Arrowheads in (I) show sites of Dpy accumulation, and their quantification is shown in (H). Number of discs analyzed = 4. Significance was determined using two-tailed t-test. (H) Quantification of the level of Dpy-YFP (+/- SD) retained within the *repo*>KDEL-RFP channel. Control, n=4; *tango1-IR*, n=4. Significance was determined using two-tailed t-test. (J-K) Live pupae expressing KDEL-RFP under the tendon cell driver *sr-gal4,* and endogenous Dpy-YFP expression. Arrowheads in (K) point to sites of Dpy accumulation. Scale bars are 25μm (A), 5μm (C), 10μm (E, G, I), and 50μm (J, K).

Figure S5 Effect of loss of *tango1* in the fat body on βPS integrin and collagen .

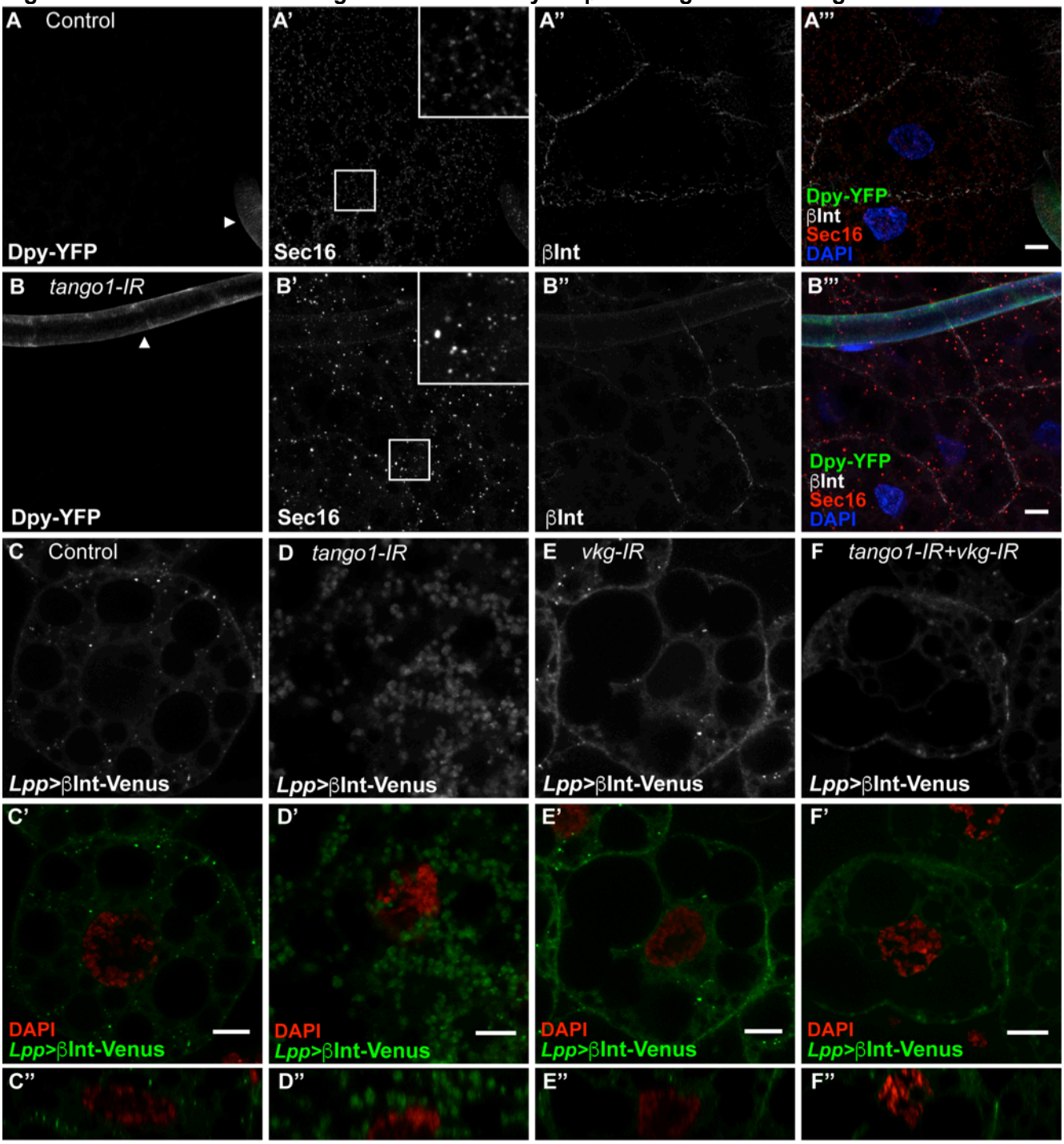

(A-B) Single z sections of fat body cells from Dpy-YFP larvae were stained for Sec16 and βPS integrin (βInt). Arrowheads point to tracheal tubes (not affected by transgenes expressed under *Lpp-gal4*) as positive control for Dpy-YFP expression. In the absence of *tango1* (B), the regular distribution of Sec16 is lost, whereas βInt is not affected. (C-F) Single z sections of fat body cells expressing βInt-Venus under *Lpp-gal4*. Control cells (C) are able to deliver βInt-Venus to the cell membrane, whereas *tango1-IR* cells (D) cannot. The absence of collagen (*vkg-IR*, E) does not affect βInt-Venus delivery. (F) Knocking down both *tango1* and *vkg* rescues membrane delivery of βInt-Venus. (C''-F'') Orthogonal views of the same cells. Scale bars are 10μm.

Figure S6. Effects of *tango1* knockdown on protein trafficking in various tissues.

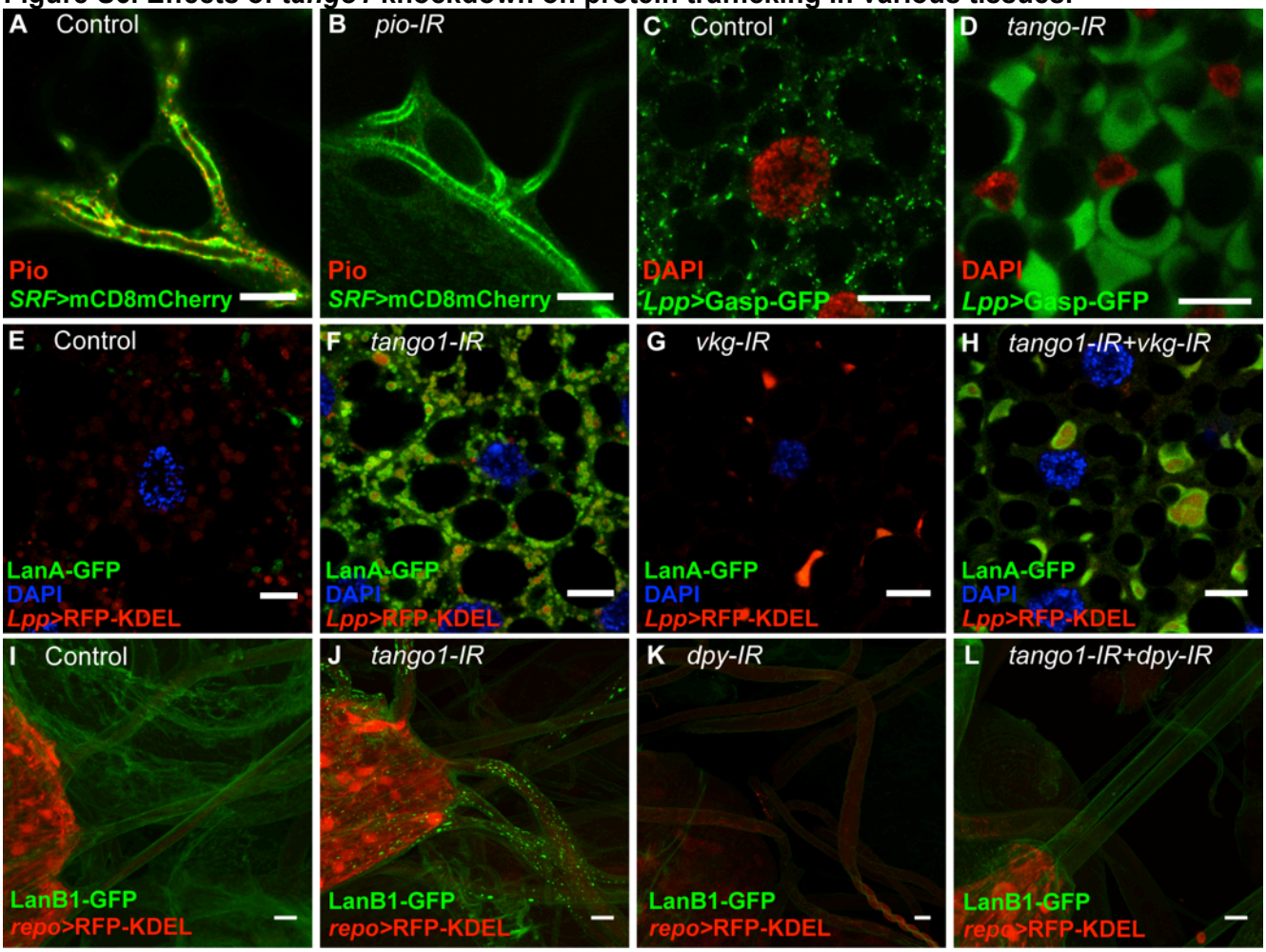

(A-B). Confocal projections of terminal cells expressing *SRF*>mCD8mCherry and stained for Pio. (A) Control cells. (B) RNAi against *pio* efficiently knocks down Pio expression. (C-D) Single z sections of fat body cells expressing Gasp-GFP under *Lpp-gal4*. Compared to control cells (A), cells expressing *tango1-IR* show high levels of diffuse cytoplasmic Gasp-GFP (B). (E-H) KDEL-RFP expression was targeted to fat body cells using *Lpp-gal4*, in animals expressing LanA-GFP under its endogenous promoter (fTRG library). LanA-GFP is retained in the ER in the absence of either Tango1 (F) or collagen (G). (I-L) KDEL-RFP expression was targeted to glial cells using the glial-specific driver *repo-gal4* in animals expressing LanB1-GFP under its endogenous promoter (fTRG library). (I) control. (J) *tango1-IR* induces LanB1-GFP retention in the ER. Whereas *dpy-IR* alone does not affect LanB1-GFP distribution (K), it suppresses the *tango1*-induced LanB1-GFP accumulation (L). Scale bars are 10μm.

Figure S7. Effects of loss of Tango1 and collagen in the fat body

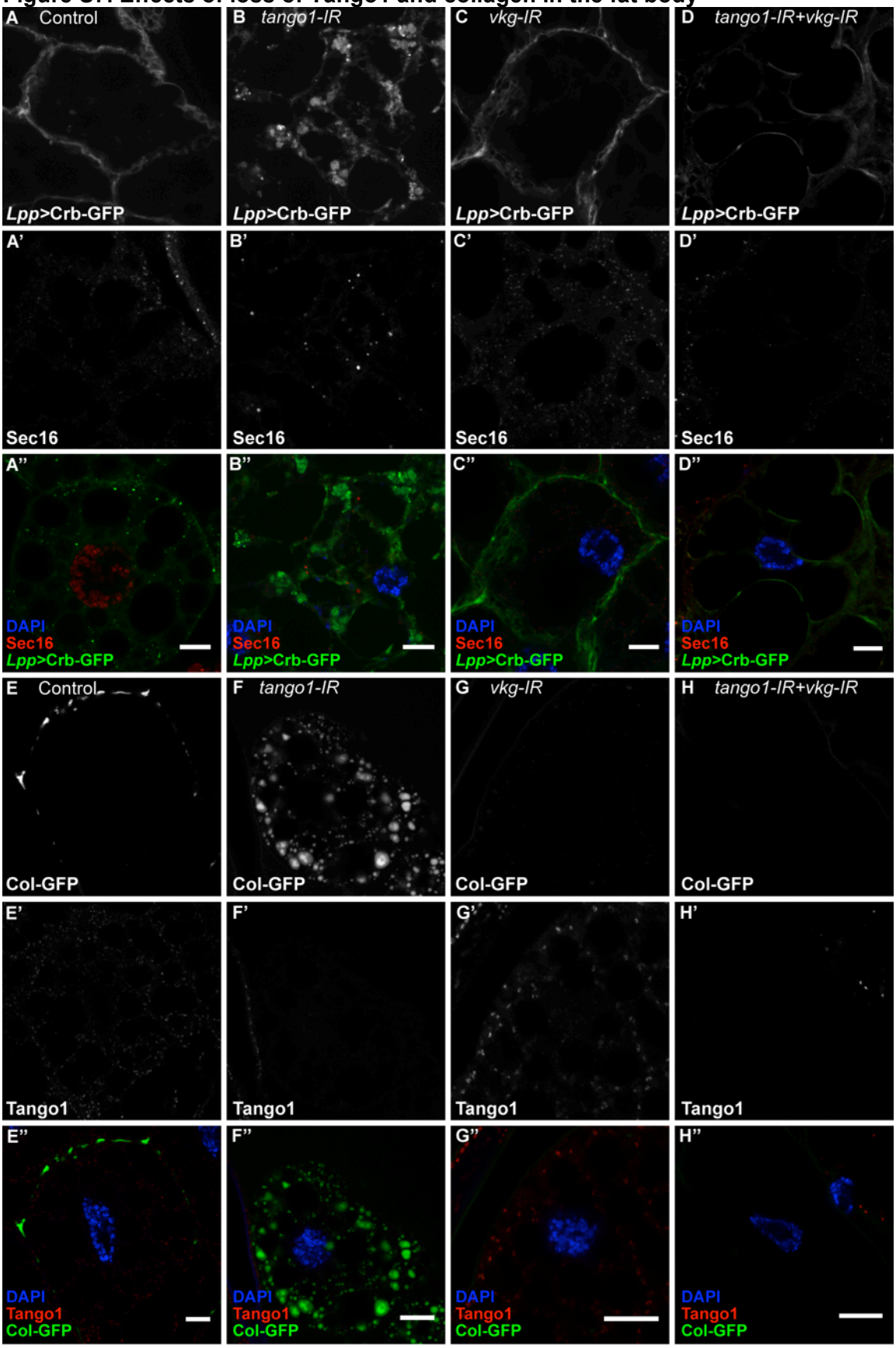

(A-D). Single z planes of fat body cells expressing Crb-GFP under *Lpp-gal4* (A-D) and stained for Sec16 (A'-D') Overlay A"-D". While control cells (A) and *vkg-IR* cells (C) traffic Crb-GFP to the cell membrane, *tango1* knockdown cells accumulate intracellular Crb-GFP (B). Transport of Crb-GFP to the cell surface is restored when both *tango1* and *vkg* are knocked down simultaneously. Sec16 distribution is aberrant in the absence of Tango1, and this is not rescued by depleting *vkg* (D). (E-H) Single z planes of fat body cells that express collagen fused to GFP and were stained for Tango1. (E) Control distribution of collagen and Tango1. (F) In the presence of *tango1-IR,* Tango1 is not detectable. (G) In the presence of *vkg-IR*, collagen-GFP is not detectable. (H) Double *tango1-IR* and *vkg-IR* does not affect silencing efficiency of either of the two proteins. Scale bars are 10μm.

Figure S8. Dependence on collagen of Laminin and SPARC secretion in fat body cells.

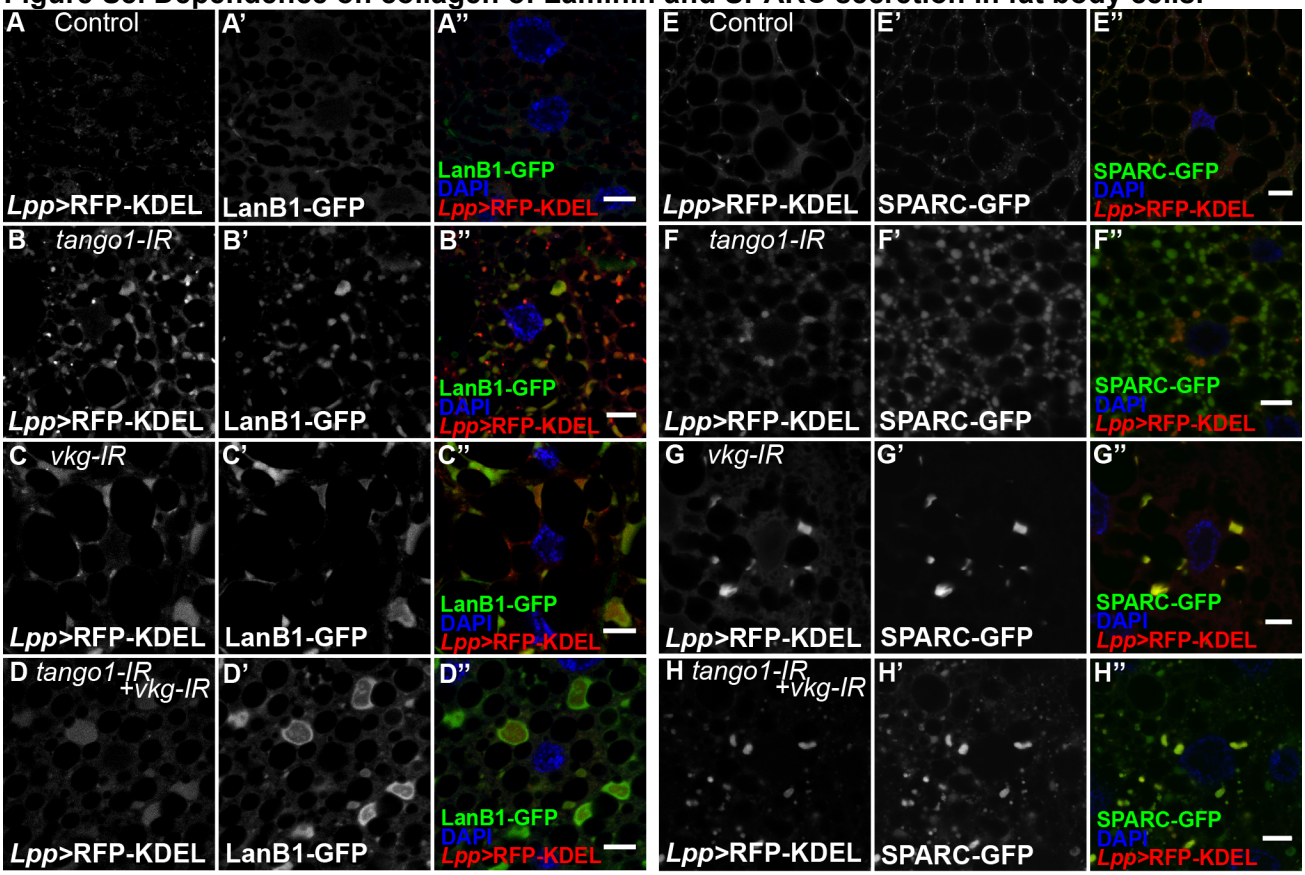

KDEL-RFP was expressed in fat body cells using *Lpp-gal4* in animals expressing LanB1-GFP (A-D) or SPARC-GFP (E-H) under their endogenous promoters (fTRG library). Both proteins are retained in the ER in the absence of Tango1 (B, F), collagen (C, G) or both (D, H). Scale bars are 10μm.

Figure S9. Laminin accumulation in *tango1*-depleted cells can be suppressed by removing Dpy.

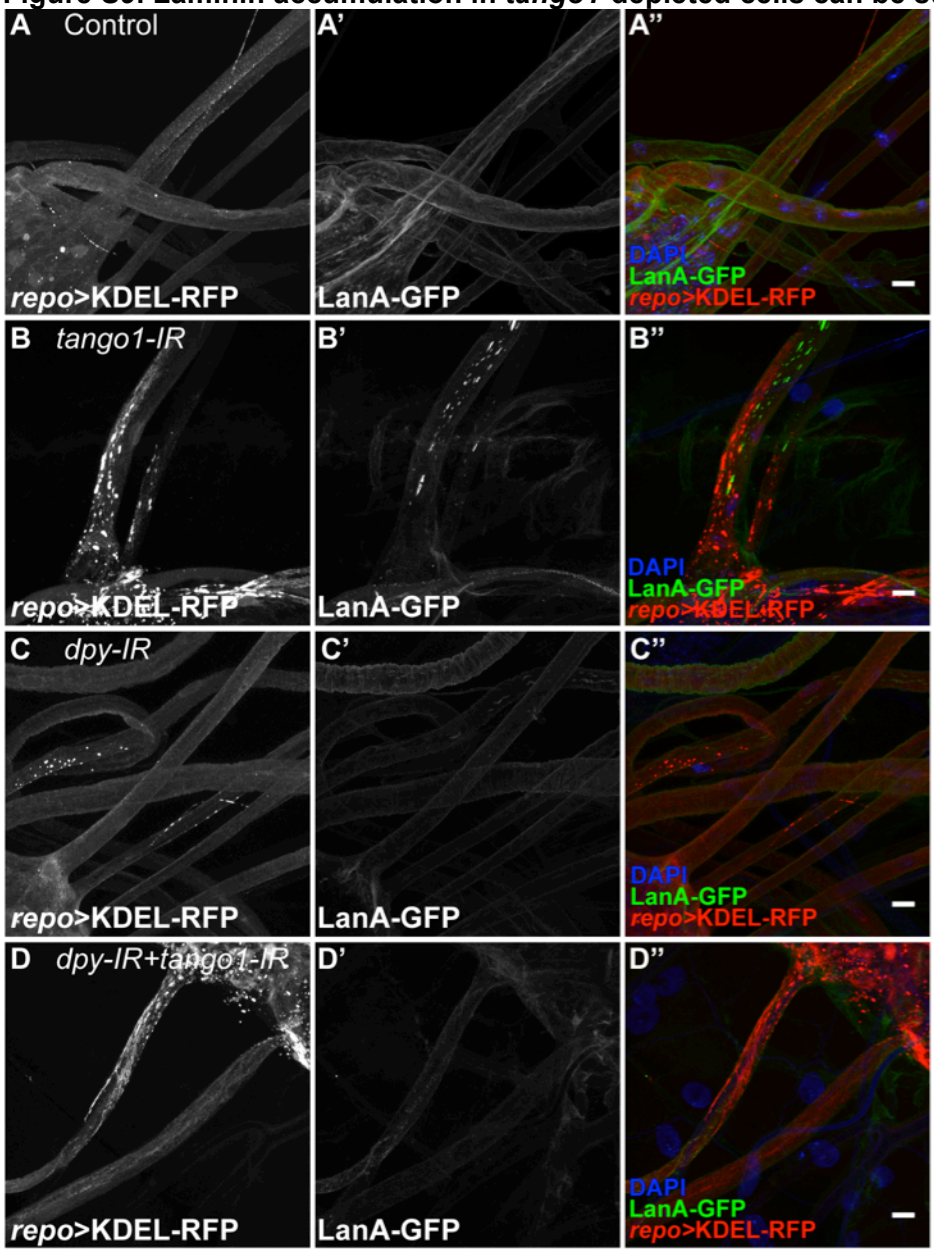

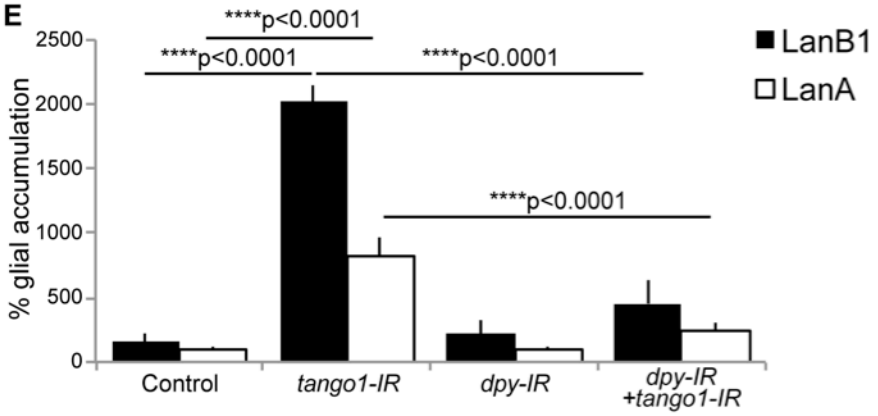

KDEL-RFP was expressed in glial cells using *repo-gal4* in animals expressing LanA-GFP under its endogenous promoter (fTRG library) in control cells (A), in cells expressing *tango1-IR* (B), *dpy-IR* (C) or both (D). *tango1-IR* induces LanA-GFP retention at the ER (B). While *dpy-IR* alone does not affect LanA-GFP distribution (C), it suppresses the *tango1*-induced LanA-GFP accumulation (D). (E) Quantification of the intracellular level of LanA and LanB1 with respect to that of control animals +/- SEM. Control, LanA n=4, LanB1 n=3; *tango1-IR*, LanA n=5, LanB1 n=3; *dpy-IR*, LanA n=6, LanB1 n=3; *tango1-IR*+*dpy-IR,* LanA n=7, LanB1 n=3. Significance was determined using one-way ANOVA and Tukey's multiple comparisons test. Scale bars are 10μm

Figure S10. Efficiency of *tango1* and *dpy* knockdown in glia and terminal cells

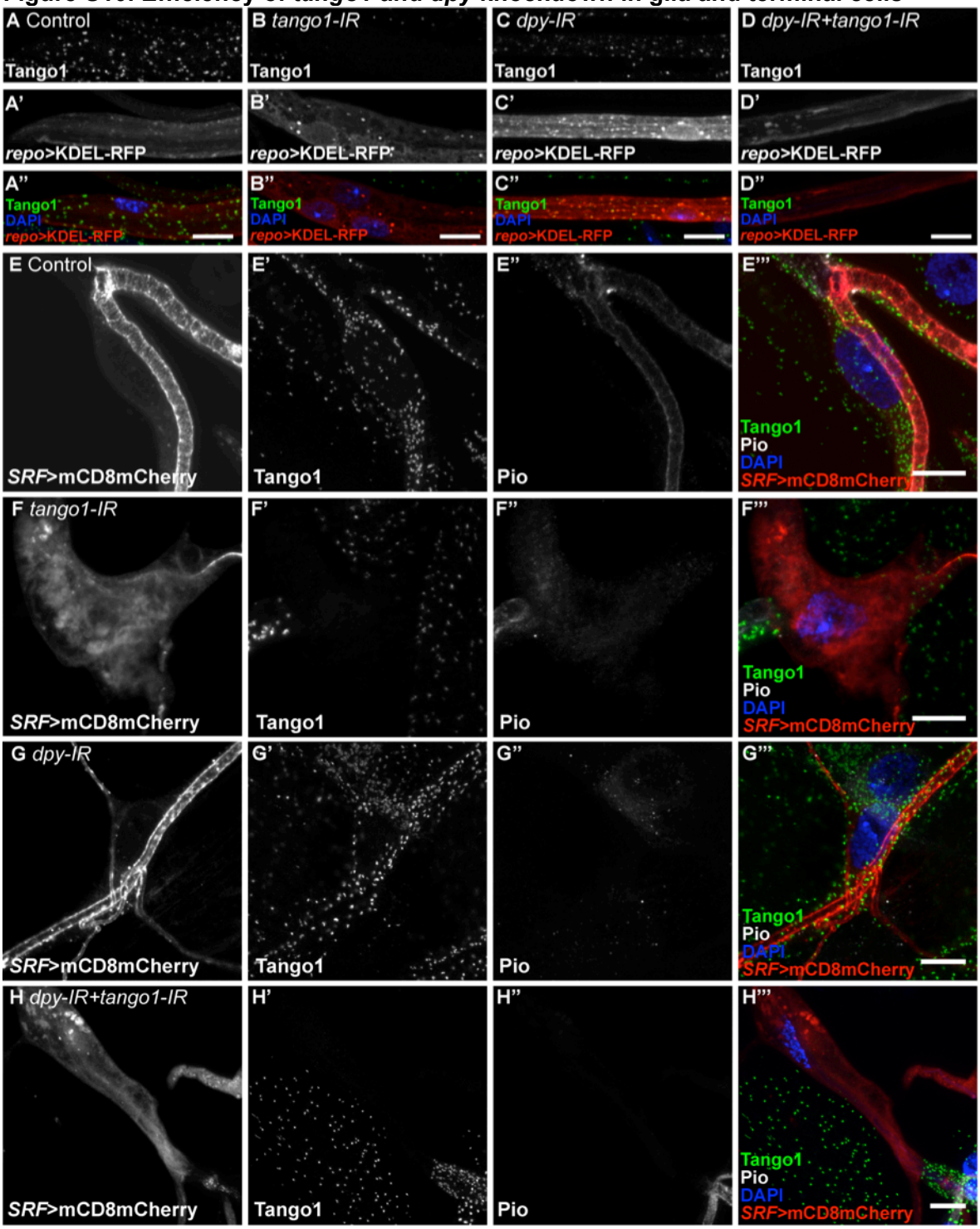

(A-D) Glial cells expressing KDEL-RFP under *repo-gal4* were stained for Tango1. Control (A) and *dpy-IR* (C) show Tango1 dotted distribution within glial cells. Tango1 is not detectable in *tango-IR* (B) and *dpy-IR, tango1-IR* (D) cells. (E-H) terminal cells expressing mCD8mCherry under *SRF-gal4* were stained for Tango1, and for Pio as a proxy for Dpy expression (Jazwinska et al., 2003). (E) Control. (F) Tango1 protein is not detectable in *tango1-IR* cells, and Pio is distributed throughout the cytoplasm. *dpy-IR* cells show normal Tango1 levels, but no detectable Pio (G). Neither Tango1 nor Pio are detectable in *tango1-IR, dpy-IR* knockdown cells (H). Scale bars are 10μm.

Figure S11. Effects of *tango1* knockdown on Calnexin and cargo accumulation.

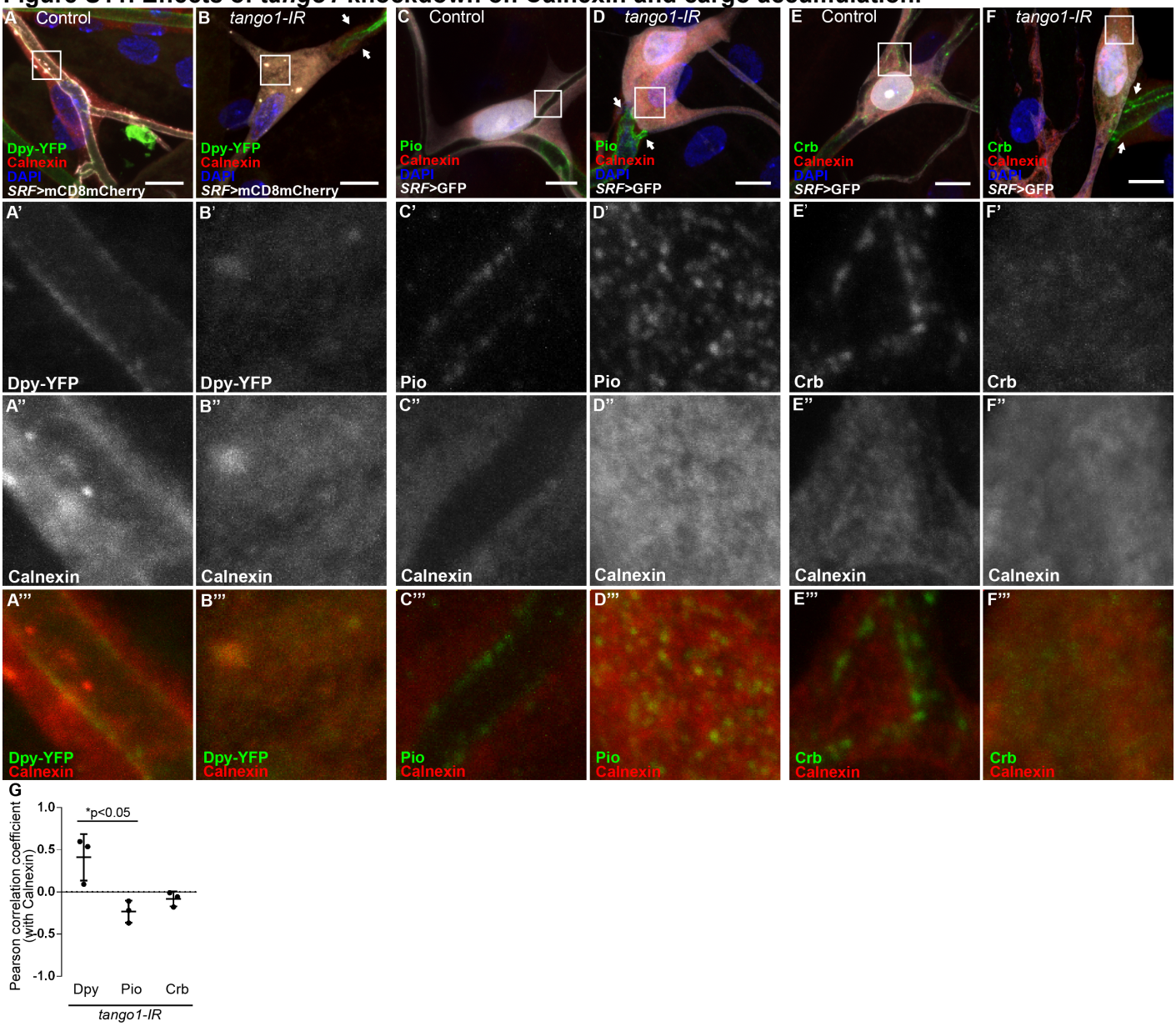

(A-B) Confocal projections of terminal cells expressing mCD8mCherry under *SRF-gal4*, endogenously tagged Dpy-YFP (A'-B') and stained for Calnexin (A''-B''). While in control cells Dpy-YFP is seen at the luminal membrane (A-A'''), in cells lacking *tango1* Dpy-YFP shows a cytoplasmic distribution that partially overlaps with Calnexin (B-B'''). (C-F) Confocal projections of terminal cells expressing GFP under *SRF-gal4* and stained for Calnexin and Pio (C-D) or Crb (E-F). While in control cells Pio and Crb localize to the luminal membrane (C-C''', E-E'''), in cells lacking *tango1* Pio and Crb show a cytoplasmic distribution that does not overlap with Calnexin (D-D''', F-F'''). Pearson correlation coefficient quantification of Calnexin with Dpy, Pio or Crb in three different cells is shown in H. Significance was determined using one-way ANOVA and Sidak's multiple comparisons test. Scale bars are 10μm.

Figure S12. Distribution of cargo proteins and Sec23 in cells lacking Tango1.

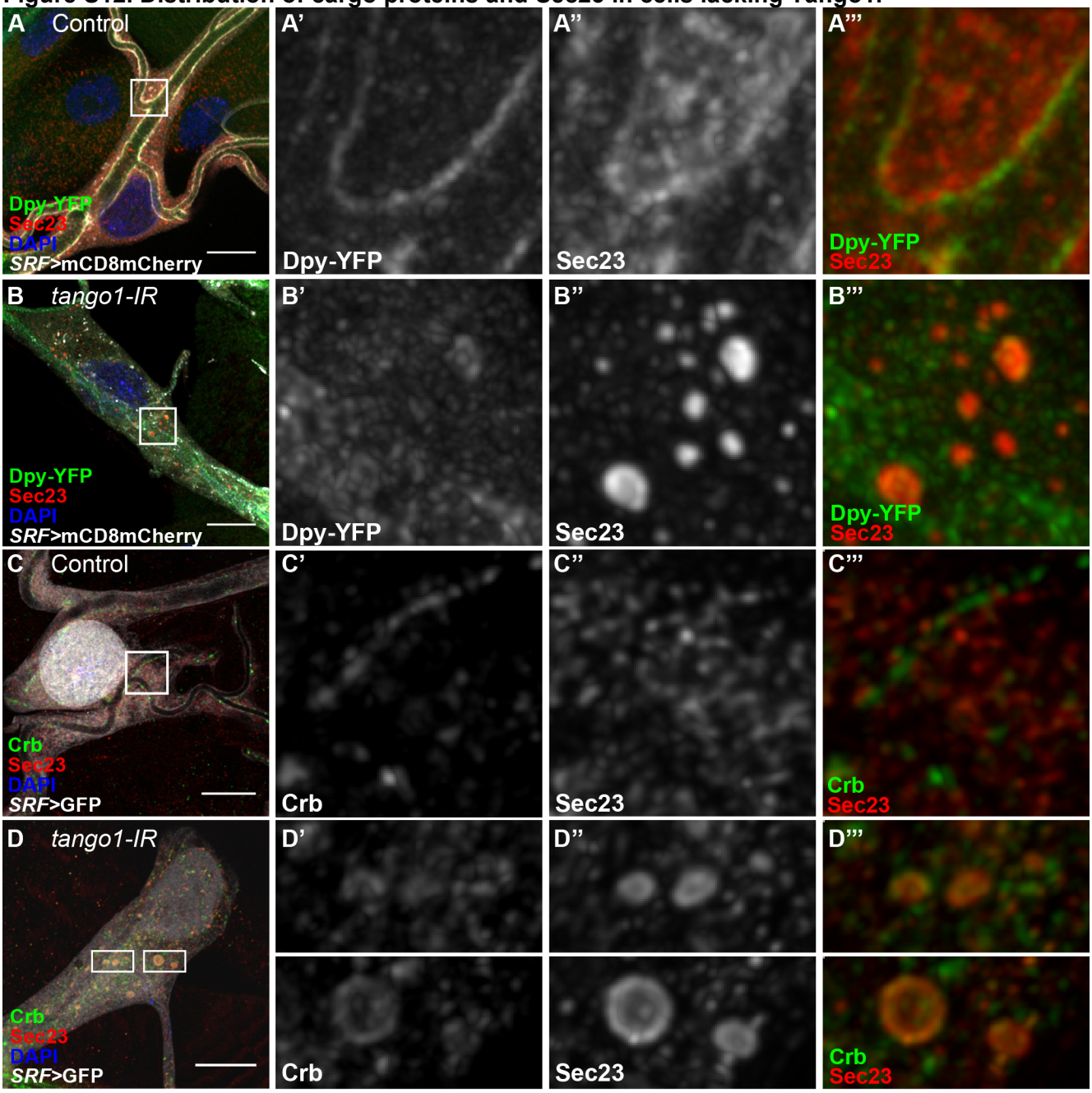

(A-B) Deconvolved confocal projections of terminal cells expressing mCD8mCherry under *SRF-gal4*, endogenously tagged Dpy-YFP (A'-B') and stained for Sec23 (A''-B''). While in control cells Dpy-YFP is seen at the luminal membrane (A-A'''), in cells lacking *tango1* Dpy-YFP shows a cytoplasmic distribution that partially overlaps with Sec23 (B-B'''). (C-D) Deconvolved confocal projections of terminal cells expressing GFP under *SRF-gal4* and stained for Sec23 and Crb. While in control cells Crb localizes to the luminal membrane (C-C'''), in cells lacking *tango1* Crb shows a cytoplasmic distribution that partially overlaps with Sec23 (D-D'''). Scale bars are 10μm.

Figure S13. Distribution of ERGIC53-GFP and Sec16 in cells lacking Tango1 and Dumpy.

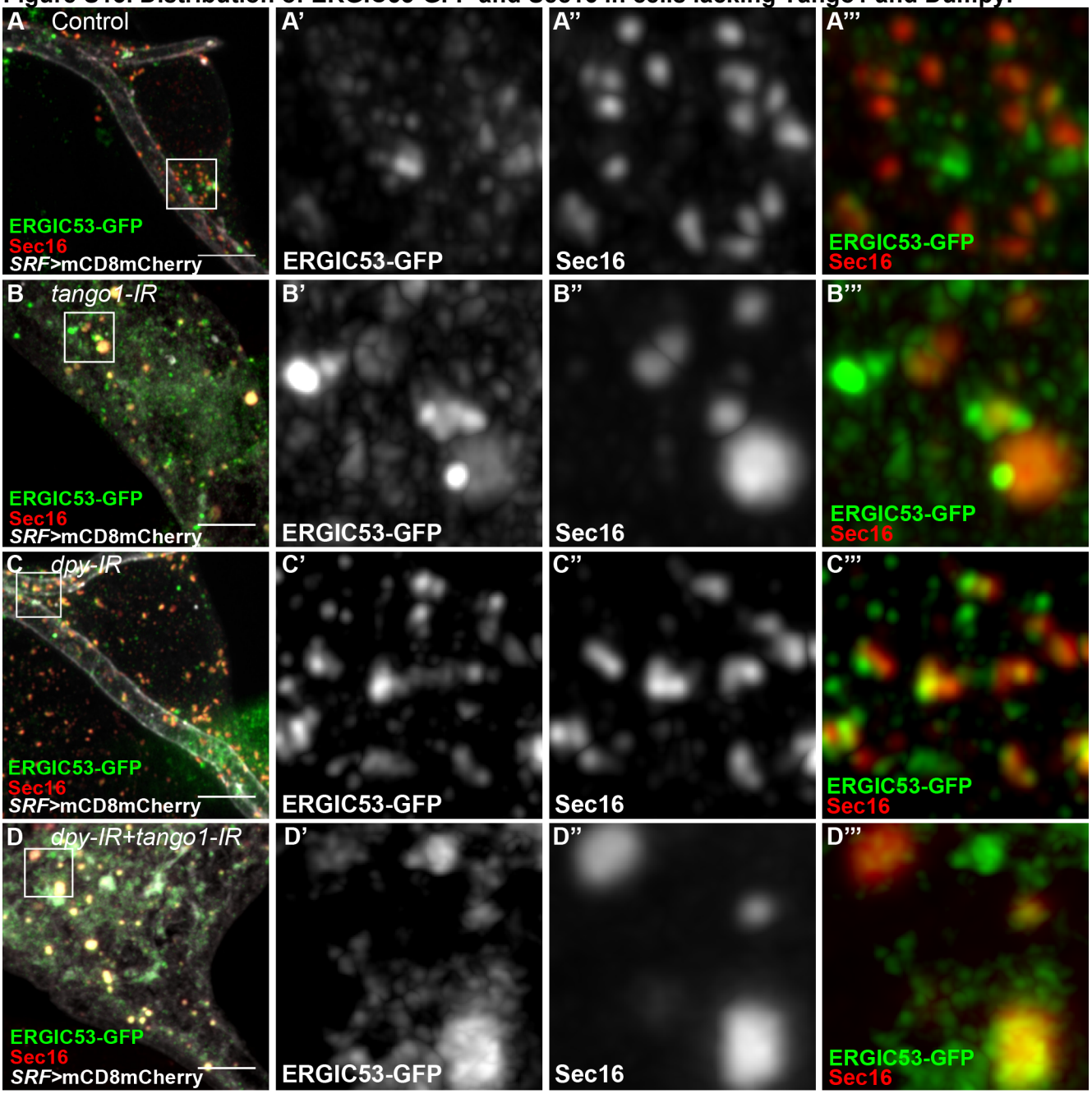

(A-B) Airyscan confocal projections of terminal cells expressing mCD8mCherry under *SRF-gal4*, from animals expressing ERGIC53-GFP under its endogenous promoter (fTRG library, A'-B') and stained for Sec16 (A''-B''). While in control and *dpy* knockdown cells ERGIC53-GFP and Sec16 are yuxtaposed and only partially overlapping (A-A''', C-C'''), in cells lacking *tango1,* ERGIC53-GFP signal is seen within the Sec16 signal (B-B'''). In double knockdown cells, ERGIC53-GFP distribution is partially rescued (D-D''').(E) Quantification of ERGIC53-GFP mean fluorescence intensity within the Sec16 spots. For each genotype, n=3 larvae. Significance was determined using one-way ANOVA and Sidak's multiple comparisons test. Scale bars are 5μm.

Figure S14. Distribution of Sec23 in cells lacking Tango1 and Dumpy.

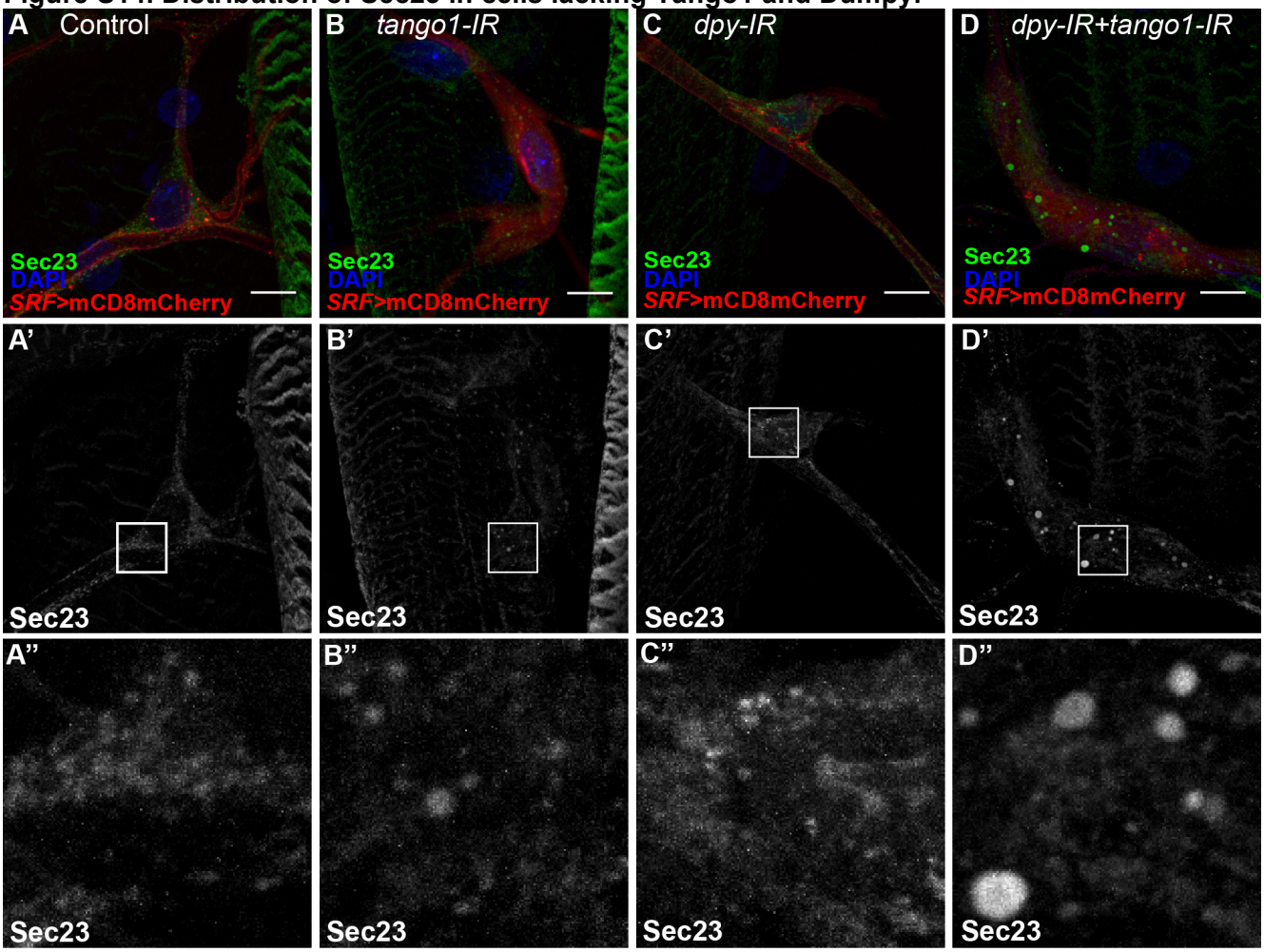

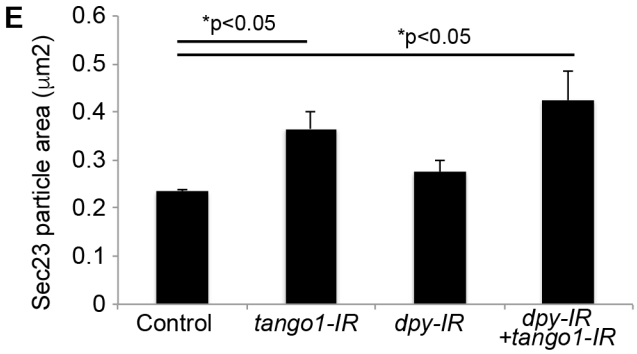

(A-D) Confocal projections of terminal cells expressing mCD8mCherry under *SRF-gal4*, stained for Sec23 (A'-D' and insets in A''-D''). While control and *dpy* knockdown cells show a homogeneous distribution of Sec23 particles (A-A'', C-C''), in cells lacking *tango1,* Sec23 forms aggregates (B-B''). Additional knockout of *dumpy* does not rescue Sec23 distribution (D-D''). (E) Quantification of Sec23 particle size. Control n=4, *tango1-IR* n=5, *dpy-IR* n=5, *dpy-IR+tango1-IR* n=6. Significance was determined using one-way ANOVA and Sidak's multiple comparisons test. Scale bars are 10μm.

References

1. Baer MM, Bilstein A, & Leptin M (2007) A clonal genetic screen for mutants causing defects in larval tracheal morphogenesis in Drosophila. *Genetics* 176(4):2279-2291.
2. Guillemin K, Williams T, & Krasnow MA (2001) A nuclear lamin is required for cytoplasmic organization and egg polarity in Drosophila. *Nat Cell Biol* 3(9):848-851.
3. Palm W*, et al.* (2012) Lipoproteins in Drosophila melanogaster--assembly, function, and influence on tissue lipid composition. *PLoS Genet* 8(7):e1002828.
4. Sarov M*, et al.* (2016) A genome-wide resource for the analysis of protein localisation in Drosophila. *Elife* 5:e12068.
5. Ray RP*, et al.* (2015) Patterned Anchorage to the Apical Extracellular Matrix Defines Tissue Shape in the Developing Appendages of Drosophila. *Dev Cell* 34(3):310-322.
6. Morin X, Daneman R, Zavortink M, & Chia W (2001) A protein trap strategy to detect GFP-tagged proteins expressed from their endogenous loci in Drosophila. *Proc Natl Acad Sci U S A* 98(26):15050-15055.
7. Pellikka M*, et al.* (2002) Crumbs, the Drosophila homologue of human CRB1/RP12, is essential for photoreceptor morphogenesis. *Nature* 416(6877):143-149.
8. Tiklova K, Tsarouhas V, & Samakovlis C (2013) Control of airway tube diameter and integrity by secreted chitin-binding proteins in Drosophila. *PLoS One* 8(6):e67415.
9. Ryoo HD, Domingos PM, Kang MJ, & Steller H (2007) Unfolded protein response in a Drosophila model for retinal degeneration. *EMBO J* 26(1):242-252.
10. Yuan L, Fairchild MJ, Perkins AD, & Tanentzapf G (2010) Analysis of integrin turnover in fly myotendinous junctions. *J Cell Sci* 123(Pt 6):939-946.
11. Schindelin J*, et al.* (2012) Fiji: an open-source platform for biological-image analysis. *Nat Methods* 9(7):676-682.
12. Jazwinska A, Ribeiro C, & Affolter M (2003) Epithelial tube morphogenesis during Drosophila tracheal development requires Piopio, a luminal ZP protein. *Nat Cell Biol* 5(10):895-901.
13. Riedel F, Gillingham AK, Rosa-Ferreira C, Galindo A, & Munro S (2016) An antibody toolkit for the study of membrane traffic in Drosophila melanogaster. *Biol Open* 5(7):987-992.
14. Vincent S, Wilson R, Coelho C, Affolter M, & Leptin M (1998) The Drosophila protein Dof is specifically required for FGF signaling. *Molecular Cell* 2(4):515-525.